Breast Tissue Density Quantification Via Digitized Mammograms

Punam K. Saha, *Member, IEEE*, Jayaram K. Udupa*, *Senior Member, IEEE*, Emily F. Conant, Dev P. Chakraborty, and Daniel Sullivan

***Abstract*—Studies reported in the literature indicate that breast cancer risk is associated with mammographic densities. An objective, repeatable, and a quantitative measure of risk derived from mammographic densities will be of considerable use in recommending alternative screening paradigms and/or preventive measures. However, image processing efforts toward this goal seem to be sparse in the literature, and automatic and efficient methods do not seem to exist. In this paper, we describe and validate an automatic and reproducible method to segment dense tissue regions from fat within breasts from digitized mammograms using scale-based fuzzy connectivity methods. Different measures for characterizing mammographic density are computed from the segmented regions and their robustness in terms of their linear correlation across two different projections—cranio-caudal and medio-lateral-oblique—are studied. The accuracy of the method is studied by computing the area of mismatch of segmented dense regions using the proposed method and using manual outlining. A comparison between the mammographic density parameter taking into account the original intensities and that just considering the segmented area indicates that the former may have some advantages over the latter.**

***Index Terms*—Fuzzy connectedness, glandular tissue, image analysis, image segmentation, mammograms.**

I. Introduction

In THE mid 1970s, studies by J. Wolfe [1], [2] suggested that an association existed between mammographic parenchymal patterns and the risk of developing breast cancer. Since then there have been many studies looking at the relationship between mammographic fibroglandular density (often referred to as just density) and the risk of developing breast cancer. Although a few studies reported no association of density with increased risk, the majority of studies have found an association between parenchymal patterns and breast cancer risk. A recent meta-analysis of all studies confirms that subjects with mammographic densities have an increased risk of breast cancer relative to those without densities. The risk increases with the density of the breast [4]. Women with dense breasts are known to have a four to sixfold increase in breast cancer risk [1], [5], [6]. Cancers are detected at later stages in dense breasts and mammographers recognize that their diagnostic accuracy is lower in such women.

The Wolfe classification was proposed many years ago to identify groups of women at high risk for breast cancer [5]. This scheme was widely used for many years, but has fallen into disuse because of several limitations. For example, interobserver variability is a problem when the radiologists' subjective assessment is used to classify the amount of density present [7]. Second, the magnitude of the increased risk has varied widely in the published studies [3]. Third, identification of this risk factor for a given woman has not altered screening recommendations [6], [8]. Computer-assisted analysis of mammographic density would provide an objective, quantitative measure of cancer risk factor. This measure will be useful in total risk analysis in several ways. First, such risk analysis could influence the choice of alternative screening paradigms such as intervals between mammograms or use of other modalities such as MRI. Second, this measure could be useful in selecting a group of women for whom the risk-benefit ratio of a potentially toxic preventive measure, such as tamoxifin, would be favorable [16], [17]. Third, this measure could be used to signal the need for more careful interpretation of a subset of mammograms. For example, double-reading might be indicated for mammograms above a certain level of density.

Image processing efforts toward this goal seem to be sparse in the literature, and automatic and efficient methods for generating this measure do not seem to exist. Boyd *et al.* [6] studied the relation between mammographic densities and breast cancer risk using both radiologist classification and computer-assisted density measurement. The computer-assisted measurement was based on interactive density thresholding using two user-selected thresholds. They observed statistically significant increases in breast cancer risk associated with increasing mammographic density in both methods. Boone *et al.* [18] developed and evaluated a computerized method of calculating a breast density index and compared this index with breast density index ranking provided by mammographers. Byng *et al.* [19] made a quantitative symmetry analysis between mammograms of different breasts of the same patient and between mammograms at different projections of the same breast via subjective classification, interactive thresholding, regional skewness measurement, and texture analysis. Ursin *et al.* [20] studied the change in mammographic densities in women participating in a trial of a gonadotropin-releasing hormone agonist (GnRHA)-based regimen for breast cancer prevention using simultaneous evaluation, expert outlining, and nonexpert computer-based thresholding methods.

Manuscript received May 17, 1999; revised May 11, 2001. This work was supported in part by the U.S. Department of the Army under Grant DAMD 179717271 and in part by the National Institutes of Health (NIH) under Grant NS 37172. The Associate Editor responsible for coordinating the review of this paper and recommending its publication was M. Giger. *Asterisk indicates corresponding author.*

P. K. Saha, E. F. Conant, and D. P. Chakraborty are with the Department of Radiology, University of Pennsylvania, Philadelphia, PA 19104 USA.

*J. K. Udupa is with the Medical Image Processing Group, Department of Radiology, University of Pennsylvania, 4th floor, Blockley Hall, 423 Guardian Drive, Philadelphia, PA 19104-6021 USA (e-mail: jay@mipg.upenn.edu).

D. Sullivan is with the National Cancer Institute-EPN-800, Rockville, MD 20852 USA.

Publisher Item Identifier S 0278-0062(01)06586-7.

They observed that all three methods yielded statistically significant reduction in densities from baseline to the 12-mo. follow-up mammogram in women on the contraceptive regimen. They found a high correlation between computer-based results and the results from the expert outlining method. Huo *et al.* [21] studied the ability of computer-extracted features, computed over a region of interest selected from the central breast region, along with age, to identify women at risk. They found that a computerized characterization of parenchymal patterns may be associated with breast cancer risk. An automatic method for segmenting the parenchymal region of a mammogram using first and second order gray-level histograms is presented in [22]. Another approach is presented in [23] for determining the volume of non fatty tissues in mammograms. Recently a computer-assisted user-interactive method to quantify mammographic density has been published [6], which concluded that quantitative classification of densities allows for the determination of more specific gradients of risk than do Wolfe's classifications.

In this paper, we describe and validate an automatic and reproducible method to quantify mammographic densities and study the accuracy of related parameters. In Section II, a brief description of the principles of the scale-based fuzzy connectedness method which forms the core of the proposed method is presented. In Section III, we describe how different parameters are automatically selected for applying fuzzy connectivity on different regions. In Section IV, we discuss the results and validate the method 1) by studying linear correlations of different area and density related parameters obtained from a set of mammograms across two projections and 2) by studying the accuracy of the method by computing the area of mismatch between the dense regions estimated by the new method and by manual outlining. A comparison between the mammographic density parameter taking into account the original intensities and that just considering the segmented area is demonstrated. Finally, we state our conclusions in Section V.

II. Scale-Based Fuzzy Connectedness Principles

The concepts described here are applicable to n-dimensional (fuzzy) digital spaces; see [24] and [25] for details. However, since our application deals with two-dimensional (2-D) images, we confine ourselves only to the 2-D case.

Most real objects have a heterogeneous material composition. Further, imaging devices have inherent limitations including spatial, parametric, and temporal resolutions. In the acquired images of objects, these introduce inaccuracies and artifacts such as noise, blurring, and background variation. The artifacts together with material heterogeneity cause the object regions to exhibit a gradation of intensity values in the image. Even if the physical object is perfectly homogeneous and is made of exactly one material, its image will exhibit a graded composition within the object regions due to artifacts. In spite of the graded composition, knowledgeable human observers usually do not have difficulties in perceiving object regions as an integrated whole. That is, image elements in these regions seem to hang together to form the object regions in spite of their gradation of values. These two notions—graded composition and hanging togetherness—must be handled properly by any segmentation method for effective, robust performance. In our methods, they are addressed by a fuzzy relation among image elements called fuzzy connectedness [24], [25]. Such a general, sound, theoretic and algorithmic framework for segmentation greatly facilitates the quick development of new segmentation applications, as we have demonstrated for fuzzy connectedness in brain image analysis [10]–[13], MRA [14], and craniofacial soft tissue display [15].

The scale-based method is briefly outlined below to the extent needed to follow our breast segmentation approach. The full details of its theory are given in [25]. We will be dealing with two object regions in our segmentation method as described in Section III. The first corresponds to the background region in the mammographic image and the second corresponds to the dense region. In the description in the rest of this section, "object region" refers to each of these regions.

Throughout we denote the digitized mammographic image, referred to as a (2-D) *scene*, by $\mathcal{C} = (C, f)$, where C denotes the pixel array, and $f(c)$ denotes the pixel value for any pixel $c \in C$. For any pixel $c \in C$, we think of c as a pair (c_1, c_2) representing the two coordinates of the center of c. The range of f is assumed to be $[L, H]$, where L and H are integers.

We define a fuzzy relation κ, called *fuzzy affinity*, on the pixel array C. This is intended to be a local relation among pixels that are nearby. The strength of this relation between any two pixels c and d in C, denoted by $\mu_\kappa(c, d)$, lies in $[0, 1]$. It consists of three components: a fuzzy adjacency component α, a component ψ based on object homogeneity, and a component ϕ based on object features. The idea is that when c and d are more adjacent, have more homogeneity of intensities, and are both very close to an expected object feature value, then c and d have high affinity. In other words, they hang together locally very strongly. α depends on how far c and d are. ψ depends on how similar the intensity values (or other features) of the pixels in a neighborhood around c are to those around d. ϕ depends on how close the intensities (or other features) of the pixels around c and those around d are to some expected values of the intensities (or other features) for the object under consideration. We denote the strengths of all these three components (all of which lie in $[0, 1]$) by $\mu_\alpha(c, d)$, $\mu_\psi(c, d)$ and $\mu_\phi(c, d)$, respectively. We describe below the functional forms utilized for these components.

Although the theory permits more general forms, in this paper, we use the following functional form for μ_α. For any pixel c, $\mu_\alpha(c, c) = 1$. Further, for any two pixels c, d, $\mu_\alpha(c, d) = 1$ if c and d differ in exactly one coordinate by one; otherwise $\mu_\alpha(c, d) = 0$. The specification of both μ_ψ and μ_ϕ requires the notion of "object scale" at every pixel in $\mathcal{C}$. The idea behind this notion is that if we can roughly estimate the size of the object structure locally at every pixel, then this information can be utilized to determine a neighborhood size around c and d for specifying μ_ψ and μ_ϕ in a way that is tuned to the object and is independent of pixel-level variation due to noise. The *object scale* $r(c)$ in $\mathcal{C}$ at any pixel c in C denotes the size (radius) of the largest disc centered at c that lies entirely in the object region in which c lies. Paradoxically, it appears that computing scale requires image segmentation. It is possible, however, to develop algorithms that give a rough estimate of object scale at every pixel based on measuring intensity homogeneity discontinuities and that do not require explicit

image segmentation. We have demonstrated in [25] that this estimation is sufficient to give a good approximation of the scale and to make the fuzzy-connectedness-based segmentation very robust to noise and pixel-level variations. For now, we assume that $r(c)$ is known at any $c \in C$. In determining the scale-based fuzzy affinity between any pixels $c, d \in C$, two digital discs, centered at c and d, denoted $B_{cd}(c)$ and $B_{cd}(d)$, both of radius $\min[r(c), r(d)]$, defined by

$$B_{cd}(c) = \{e \in C \,|\, ||c-e|| \le \min[r(c), r(d)]\} \quad (1)$$

$$B_{cd}(d) = \{e \in C \,|\, ||d-e|| \le \min[r(c), r(d)]\} \quad (2)$$

where $||\cdot||$ denotes the Euclidean distance, are utilized.

For defining μ_ψ, consider any two pixels $c, d \in C$ such that $\mu_\alpha(c, d) > 0$. Consider any pixels $e \in B_{cd}(c)$ and $e' \in B_{cd}(d)$ such that they represent the corresponding pixels within $B_{cd}(c)$ and $B_{cd}(d)$; that is, $c-e = d-e'$. We will define two weighted sums $D^+(c, d)$ and $D^-(c, d)$ of the differences of intensities between the two discs as follows. Let

$$\delta^+_{cd}(e, e') = \begin{cases} f(e) - f(e'), & \text{if } f(e) - f(e') > 0, \\ 0, & \text{otherwise,} \end{cases} \quad (3)$$

$$\delta^-_{cd}(e, e') = \begin{cases} f(e') - f(e), & \text{if } f(e) - f(e') < 0, \\ 0, & \text{otherwise.} \end{cases} \quad (4)$$

Then

$$D^+(c, d) = \sum_{\substack{e \in B_{cd}(c) \\ e' \in B_{cd}(d) \\ \text{s.t. } c-e=d-e'}} [1 - G_{0,\, m_\psi + 3\sigma_\psi}(\delta^+_{cd}(e, e'))] \cdot G_{0,\, \min[r(c), r(d)]}(||c-e||) \quad (5)$$

$$D^-(c, d) = \sum_{\substack{e \in B_{cd}(c) \\ e' \in B_{cd}(d) \\ \text{s.t. } c-e=d-e'}} [1 - G_{0,\, m_\psi + 3\sigma_\psi}(\delta^-_{cd}(e, e'))] \cdot G_{0,\, \min[r(c), r(d)]}(||c-e||) \quad (6)$$

where

- "s.t." "such that";
- $G_{m,\sigma}$ unnormalized Gaussian with mean m and standard deviation σ;
- m_ψ and σ_ψ expected mean and standard deviation of intensity differences between all pairs of adjacent pixels within the object region, respectively;
- $||c-e||$ represents the distance between c and e.

We will describe in the next section how these parameters are estimated for breast images.

The connection of the above equations to the homogeneity-based affinity μ_ψ is as follows. There are two types of intensity variations surrounding c and d—intraobject and interobject variations. The intraobject component is generally random, and therefore, is likely to be near zero overall. The interobject component, however, has a direction. It either increases or decreases along the direction given by $c-d$, and is likely to be larger than the intraobject variation. It is reasonable, therefore, to assume that the smaller of $D^+(c, d)$ and $D^-(c, d)$ represents the intraobject component and the other represents the combined effect of the two components. (Note that when the values of δ^+_{cd} [respectively, δ^-_{cd}] are small, $D^+(c, d)$ [respectively, $D^-(c, d)$] also becomes small.) If there is a slow background component of variation, within the small neighborhood considered, this component is unlikely to cause a variation comparable to the interobject component. This strategy leads us to the following functional form for μ_ψ

$$\mu_\psi(c, d) = 1 - \frac{|D^+(c, d) - D^-(c, d)|}{\sum_{e \in B_{cd}(c)} G_{0,\, \min[r(c), r(d)]}(||c-e||)}. \quad (7)$$

Note that $|D^+(c, d) - D^-(c, d)|$ represents the degree of local inhomogeneity of the regions containing c and d. Its value is low when both c and d are inside an (homogeneous) object region. Its value is high when c and d are in the vicinity of (or across) a boundary. The denominator in (7) is a normalization factor.

For completing the specification of μ_ψ, the values of three parameters $r(c)$, m_ψ and σ_ψ need to be determined. The method of estimating $r(c)$ is independent of the type of object region to be segmented and will be described later in this section. The method of estimating m_ψ and σ_ψ is specific to the object region and will be explained in Sections III-A and III-B.

For defining the object-feature-based affinity, μ_ϕ, we first compute scale-based filtered intensity value at c that takes into account the disc $B_r(c)$ defined by

$$B_r(c) = \{e \in C \,|\, ||c-e|| \le r(c)\}. \quad (8)$$

The filtered intensity value at any $c \in C$ is given by

$$f_a(c) = \frac{\sum_{e \in B_r(c)} f(e) G_{0,\, r(c)}(||c-e||)}{\sum_{e \in B_r(c)} G_{0,\, r(c)}(||c-e||)}. \quad (9)$$

Depending on whether the object of interest is darker or lighter, we define the following function utilized in defining μ_ϕ

Object is darker:

$$W_\phi(c) = \begin{cases} 1, & \text{if } f_a(c) < m_\phi \\ G_{m_\phi, \sigma_\phi}(f_a(c)), & \text{otherwise} \end{cases} \quad (10)$$

Object is lighter:

$$W_\phi(c) = \begin{cases} G_{m_\phi, \sigma_\phi}(f_a(c)), & \text{if } f_a(c) < m_\phi \\ 1, & \text{otherwise.} \end{cases} \quad (11)$$

In both cases, m_ϕ and σ_ϕ represent the expected mean and standard deviation of the intensities in the object region, respectively. Finally, the following functional form is used for μ_ϕ:

$$\mu_\phi(c, d) = \begin{cases} 1, & \text{if } c = d \\ \min[W_\phi(c), W_\phi(d)], & \text{otherwise.} \end{cases} \quad (12)$$

For completing the specification of μ_ϕ, the values of three parameters $r(c)$, m_ϕ and σ_ϕ need to be determined. The method of estimating $r(c)$ is presented below. The method of estimating m_ϕ and σ_ϕ is specific to the type of object region to be segmented and will be explained in Sections III-A and III-B. Finally, the three components of affinity are combined as follows to define the scale-based fuzzy affinity, μ_κ

$$\mu_\kappa(c, d) = \mu_\alpha(c, d) \sqrt{\mu_\psi(c, d) \mu_\phi(c, d)}. \quad (13)$$

We now describe an algorithm for estimating object scale at every pixel. For a disc $B_k(c)$ of any radius k [see (8)] centered at c, we define a fraction, $FO_k(c)$, that indicates the fraction of the disc boundary occupied by a region in which the scene is sufficiently homogeneous with c, by

$$FO_k(c) = \frac{\sum_{d \in B_k(c) - B_{k-1}(c)} G_{0, m_\psi + 3\sigma_\psi}(|f(c) - f(d)|)}{|B_k(c) - B_{k-1}(c)|}. \quad (14)$$

Here, $|B_k(c) - B_{k-1}(c)|$ denotes the number of pixels in $B_k(c) - B_{k-1}(c)$. We define $B_0(c)$ to be simply the set $\{c\}$. The algorithm for object scale estimation (OSE) is summarized below. The algorithm iteratively increases the disc radius k by 1, starting from 1, and checks for the fraction of the object $FO_k(c)$ containing c that is contained on the disc perimeter. The first time when this fraction falls below a pre-selected threshold t_s, we consider that the disc enters into an object region different from that to which c belongs. Following the arguments in [25], we have used $t_s = 0.85$:

Algorithm OSE
Input: $\mathcal{C}$, $c \in C$, m_ψ, σ_ψ, a fixed threshold t_s.
Output: $r(c)$.
begin
  set $k = 1$;
  while $FO_k(c) \geq t_s$ *do*
    set k to $k+1$;
  endwhile;
  set $r(c)$ to k;
  output $r(c)$;
end

The notion of pixel affinity captures the local hanging-togetherness property of pixels. The notion of fuzzy connectedness expands this into a global phenomenon as follows. Consider any two pixels c and d (not necessarily nearby) in C. (Note that when c and d are far apart, their affinity is zero.) Consider any path (i.e., a sequence of nearby pixels) starting from c and ending in d. We define a "strength of connectedness" of this path as simply the smallest affinity (weakest link) along the path between a pair of successive pixels in the path. Fuzzy connectedness is a global fuzzy relation, denoted K, on C. The strength of this relation between c and d (not necessarily nearby), denoted $\mu_K(c, d)$, is the largest of the strength of connectedness of *all possible* paths between c and d. A scale-based fuzzy connected object of $\mathcal{C}$ of strength θ, for any $\theta \in [0, 1]$, that contains a specified pixel o in C is a subset O of pixels of C. O is such that, for any two pixels c, d in O, $\mu_K(c, d) \geq \theta$, and for any pixel e not in O, $\mu_K(c, e) < \theta$. Given $\mathcal{C}$, o, θ and a scale-based affinity relation κ, finding O requires the computation of the strength of connectedness of literally all possible paths between each pair of pixels in the set of all possible pairs of pixels in C. However, the theory leads to practically viable algorithms [24], [25] of far less complexity that are based on dynamic programming. We make use of these algorithms in our application.

For any scene $\mathcal{C} = (C, f)$, any fuzzy affinity κ, any pixel o in C, we define the *fuzzy connectivity scene* of $\mathcal{C}$ with respect to o to be the scene $\mathcal{C}_{Ko} = (C, f_{Ko})$, where for any $c \in C$, $f_{Ko}(c) = \mu_K(o, c)$. That is, the value assigned to any pixel c in $\mathcal{C}_{Ko}$ is the strength of connectedness of c and o. We generalize this definition from a single pixel o to a set of pixels X by setting $f_{KX}(c) = \max_{x \in X}\{\mu_K(x, c)\}$. That is, in the fuzzy connectivity scene $\mathcal{C}_{KX} = (C, f_{KX})$ of $\mathcal{C}$ with respect to X, any pixel c is assigned a value $f_{KX}(c)$ that is the maximum of the strength of connectivity of c with the elements of X. Connectivity scenes are what are output by the fuzzy connectedness algorithms [24], [25]. Upon thresholding them, we get the segmented fuzzy objects.

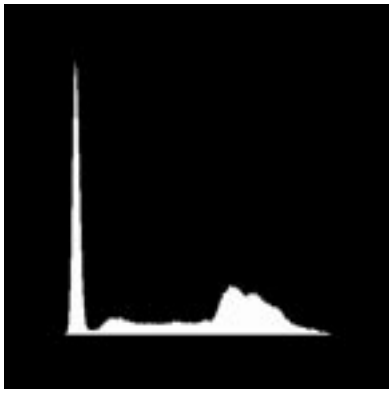

Fig. 1. A typical mammographic intensity histogram.

III. Density Quantification

Our method of mammographic density quantification consists of the following steps: 1) segmentation of the breast region from background; 2) segmentation of fat and dense regions within the breast; 3) estimation of the parameters representing quantified density. These are described in separate subsections below.

A. Segmentation of Breast from Background

At the very beginning, using 3DVIEWNIX [26] supported live-wire [27] tools, regions corresponding to pectoral muscles are interactively excluded when those are projected on to the scene. This tool takes help from the operator in recognizing where the pectoral muscles are in the image but does the delineation of their boundary automatically. In this fashion, subjectivity is minimized. In the entire process of density quantification, this is the only step requiring operator intervention, if pectoral muscles appear in the mammographic projection. Scale-based fuzzy connectivity is used for segmenting the breast region from the background. Our approach will be to segment the background region rather than the breast region. To do this, we need to 1) determine the values of the parameters m_ψ, σ_ψ, m_ϕ, and σ_ϕ for the background and 2) specify a set of pixels in the background region. These are accomplished automatically as described below.

In this study, we have utilized 120 mammograms from 60 patients, each in two projections, MLO and CC. Studying all the 120 mammograms, we found that intensity histograms of mammograms always contain a prominent peak at low intensities, and this mode corresponds to the background. A typical histogram is shown in Fig. 1.The first prominent peak in the histogram is detected and the intensity m_ϕ corresponding to this peak is considered as the mean background intensity. Observing

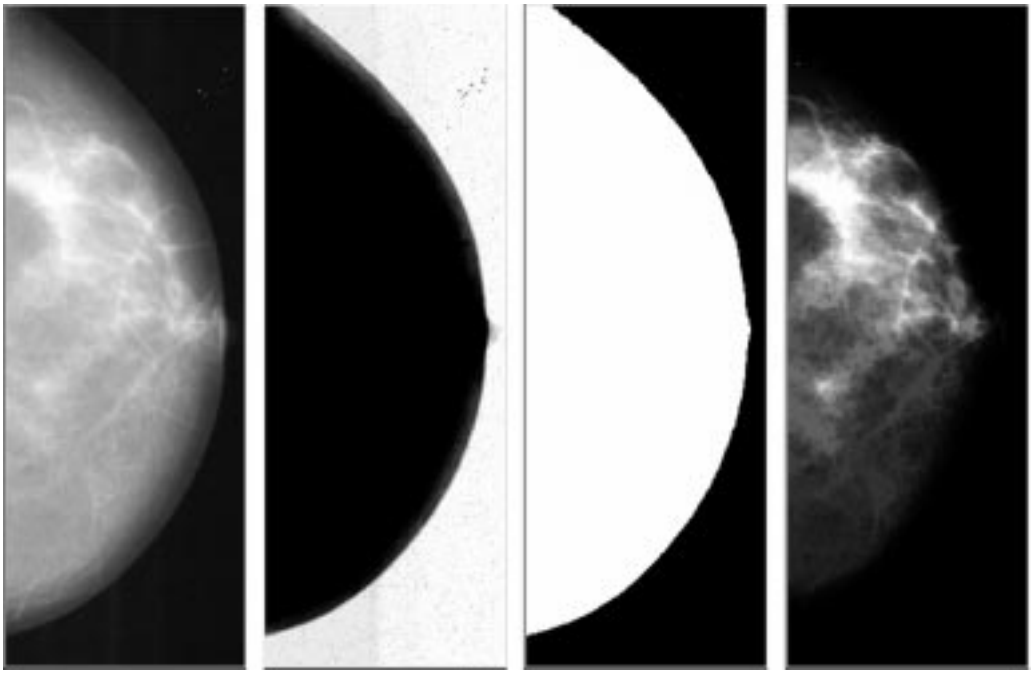

(a) (b) (c) (d)

Fig. 2. (a) An original mammographic scene of a patient's breast at CC projection. (b) Scale-based fuzzy connectivity scene for the background. (c) Segmented breast region. (d) Scale based fuzzy connectivity scene for the dense region.

that this part of the histogram is roughly symmetric about m_ϕ, the standard deviation of background intensities σ_ϕ is computed as the root-mean-squared distance of the intensities from m_ϕ as follows. Let $h(i)$ represent the number of pixels in the mammographic scene with intensity i (i.e., $h(i)$ is the height of the histogram at i). Then, σ_ϕ is determined as follows:

$$\sigma_\phi = \sqrt{\frac{\sum_{L \le i \le m_\phi} (i - m_\phi)^2 h(i)}{\sum_{L \le i \le m_\phi} h(i)}}. \tag{15}$$

In this application, since the object of interest (i.e., the mammographic background) is darker, we use the functional form of (10) for computing object-feature-based affinity. Instead of an operator painting pixels in the background region for training, the set of pixels in $\mathcal{C}$ satisfying $L \le f(c) \le m_\phi + 3\sigma_\phi$ is utilized for estimating the parameters m_ψ and σ_ψ for homogeneity-based affinity μ_ψ. m_ψ and σ_ψ are taken to be simply the mean and the standard deviation of intensity differences between all pairs of adjacent pixels in this set.

During digitization, all mammograms were oriented so that the top–right and the bottom–right corners always lie in the background. (This was standardized for both left and right breasts.) These two corner pixels are used to form the reference set X for scale-based fuzzy connectedness processing. Fig. 2(b) shows the connectivity scene obtained for the mammogram at CC projection shown in Fig. 2(a). As shown in Fig. 2(b), there is very good contrast between the background and the breast region in this connectivity scene. We discard connectivity strengths greater than half the maximum strength and keep the lower half as the zone for the breast region. This zone, however, often includes high noise pixels and markers in the background often used during mammography. To eliminate these pixels, the leftmost one-pixel in the middle row in the thresholded connectivity scene is chosen as the reference pixel and the hard connected component containing this pixel is found as the breast region. Fig. 2(c) shows the hard segmented breast region for the original mammogram of Fig. 2(a). This method has worked correctly and automatically in all studies we have analyzed so far.

B. Segmentation of Fat and Dense Regions

Our strategy here is to segment the dense region as a set of fuzzy connected objects. The segmentation operation is confined to the breast region. The fat region thus gets defined indirectly as the complement of the dense region in the breast. For this segmentation, as in breast segmentation, we need to specify the values of parameters m_ψ, σ_ψ, m_ϕ, and σ_ϕ for the dense region as well as a few pixels as the starting information in the dense region.

Our approach to computing the parameters will be as for the segmentation of the breast region; to determine automatically a set of pixels that are definitely in the dense region and then to estimate the parameters from the intensity distribution within this set of pixels. In this application, since the object of interest (i.e., the dense regions) is lighter, we use the functional form of (11) for computing object-feature- based affinity μ_ϕ. To determine a set of pixels in the dense region, the largest intensity value MAX is determined by ignoring the upper 0.1 percentile of intensity in the histogram of the breast region. Similarly, the smallest intensity value MIN is determined by ignoring the lower 0.1 percentile of intensity. We then select within the breast the set of

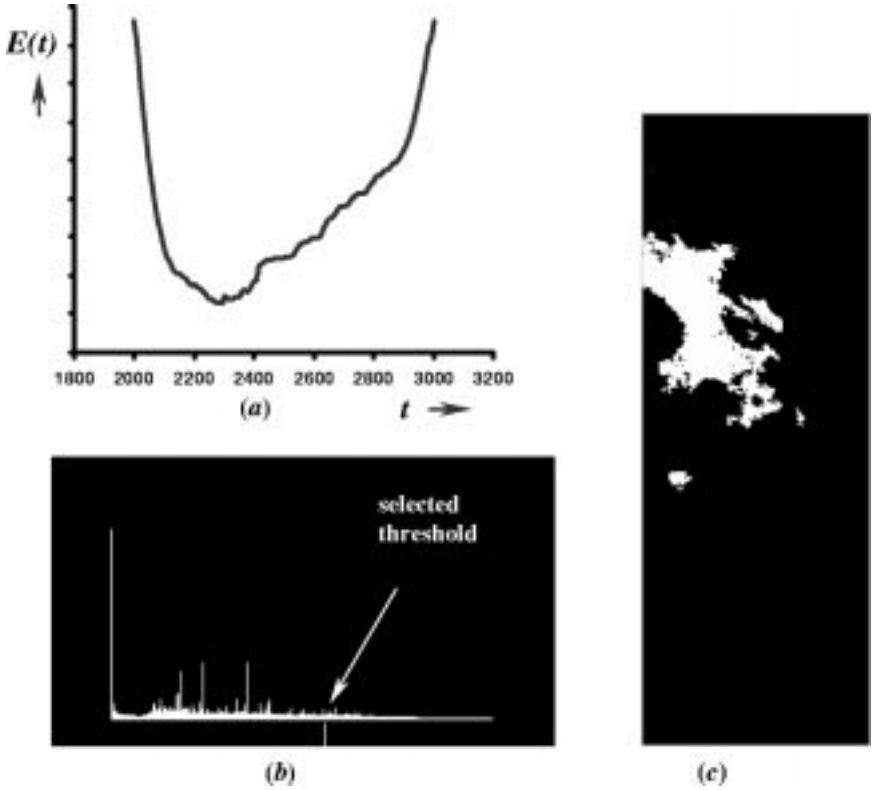

Fig. 3. (a), (b) Threshold energy and connectivity strength distributions for the connectivity scene of Fig. 2(d). (c) Segmented dense region using automatic thresholding.

pixels having intensity not less than MIN $+ 0.75$(MAX–MIN) for estimating the parameters. Specifically, we take the mean and standard deviation of the intensities of the pixels in this set as the values of m_ϕ and σ_ϕ. Further, we take the mean and standard deviation of intensity differences between all pairs of adjacent pixels in this set as the values of m_ψ and σ_ψ. Finally, the set of pixels in the breast region with intensity greater than MIN $+ 0.85$(MAX–MIN) is used as the set of reference pixels. Fig. 2(d) shows the scale-based fuzzy connectivity scene obtained for the dense region for the original mammogram in Fig. 2(a). In the next section, we describe an automatic threshold selection method that is applied to the fuzzy connectivity scene for the dense region for a segmentation of the breast region into dense and fatty regions.

C. Automatic Threshold Selection

The connectivity scene is an image in which pixels hanging together strongly with the reference pixels supposedly all belong to the same object region [24]. It is usually easy to segment the object region by thresholding the connectivity scene even if the original scene is not amenable for thresholding. This property of fuzzy connectedness is demonstrated in [24] and a quantitative validation is presented in [25]. In the past, in other applications utilizing fuzzy connectedness [10], [13]–[15], we have used fixed thresholds on connectivity scenes. In this application, we found that fixing the connectedness threshold is not always satisfactory, although each connectivity scene is still far more amenable to thresholding than the original. With this as the motivation, we developed an automatic threshold selection strategy for connectivity scenes, building on the idea of homogeneity-based affinity described in the previous selection but as applied to the connectivity scene.

To select the best threshold, the method minimizes an energy function computed by considering spatial arrangements of pixel intensities within each region and across regions. We emphasize that the processing is now confined to the breast region. The basic idea is as follows. Every threshold divides the scene into two regions. A second order statistic, threshold energy, of local disagreements in the scene stemming from this partitioning is estimated and is used as a criterion for optimizing the threshold. Threshold energy characterizes the goodness (rather, badness) of a particular threshold and is defined as follows. Let B denote the set of pixels in the segmented breast region. We define two fuzzy relations ρ and $\overline{\rho}$, respectively called *likeliness of belonging to the same object* and *likeliness of belonging to different objects*, on the pixels in B. The strengths of both these relations between any two pixels c and d in B depend on 1) how far c and d are; and on 2) how similar the intensity values (or other features) of the pixels in the circular neighborhood around c are to those around d. As discussed in Section II, the size of the circular neighborhoods around c and d depends on the object scales at c and d. In fact the criterion in 2) is the measure of homogeneity-based affinity μ_ψ between c and d. Two controlling parameters (indicating expected object homogeneity) are required to calculate the value of μ_ψ as described earlier. These two parameters are estimated as the mean and the standard deviation of intensity differences of all pairs of adjacent pixels in the region with pixel intensities (connectedness values) falling in the upper half of the histogram of the connectivity scene. The strength of

the fuzzy relation "likeliness of belonging to the same object" between two pixels $c,\ d \in B$, denoted $\mu_\rho(c,\ d)$, is then defined as follows:

$$\mu_\rho(c,\ d) = \mu_\alpha(c,\ d)\frac{\sum\limits_{\substack{a,\ b\in B\ \text{s.t.}\\ \mu_\psi(a,\ b)\le\mu_\psi(c,d)}} \mu_\alpha(a,\ b)}{\sum\limits_{a,\ b\in B}\mu_\alpha(a,b)}. \quad (16)$$

The strength of the fuzzy relation "likeliness of belonging to different objects" between two pixels $c,\ d \in B$, denoted $\mu_{\overline{\rho}}(c,\ d)$, is defined as follows

$$\mu_{\overline{\rho}}(c,\ d) = \mu_\alpha(c,\ d)\left(1 - \frac{\sum\limits_{\substack{a,\ b\in B\ \text{s.t.}\\ \mu_\psi(a,\ b)\le\mu_\psi(c,d)}} \mu_\alpha(a,\ b)}{\sum\limits_{a,\ b\in B}\mu_\alpha(a,b)}\right). \quad (17)$$

Let $f_p(c,\ d,\ t)$ denote a predicate that takes a value 1 when the pixels $c,\ d$ belong to the same object at the threshold t and zero otherwise. Then the threshold energy $E(t)$ is determined as follows:

$$E(t) = \sum_{c,\ d\in B} f_p(c,\ d,\ t)\mu_\rho(c,\ d) + (1 - f_p(c,\ d,\ t))\mu_{\overline{\rho}}(c,\ d). \quad (18)$$

In words, $E(t)$ expresses the level of concordance between the two regions resulting by applying the threshold t to the connectivity scene. Finally, the threshold for which $E(t)$ is minimum (indicating minimum concordance or maximum discordance between the two regions) is selected as the optimum threshold. For the fuzzy connectivity scene of Fig. 2(d), the distribution of $E(t)$ is shown in Fig. 3(a), while Fig. 3(b) shows the location of the optimum threshold on the histogram of the connectivity scene of Fig. 2(d). The segmented binary scene is shown in Fig. 3(c).

D. Density Quantification

From the original scene and the segmented fat and dense regions, the following parameters are computed.

TG: Total density within the breast region defined as the sum of intensities of pixels in the segmented dense region.
TF: Total fat within the breast region defined as the sum of intensities of pixels in the segmented fat region.
AB: Total area of breast defined as the number of pixels in the segmented breast region.
AG: Total area of density within the breast region defined as the number of pixels in the segmented dense region.
AF: Total area of fat within the breast region defined as the number of pixels in the segmented fat region.
AvF: Average pixel intensity within the fat area defined by TF/AF.

The following parameters, some of which are derived from the above, which may be more meaningful, are actually used in our testing: TG, TG/TF, TG/AvF, TG/AB, AG, AG/AF, and AG/AB. Linear correlations of each of these parameters across two different projections (CC and MLO) were tested for all 60 studies.

IV. Results and Discussion

The method has been tested in two ways: 1) by studying correlation of each density parameter computed from patients' mammograms at two different projections and 2) by studying the accuracy of the method in terms of the area of mismatch between dense regions segmented by the new method and by manual outlining. We chose the first experiment to validate our method following the studies in [19] wherein the authors have demonstrated a similarity of quantitative measures derived from mammographic images at different projections. In their study, interactive density thresholding by radiologist readers was used to delineate mammographic dense regions. Further, we demonstrate that fixed thresholding is not a good choice for delineating mammographic dense regions. We also demonstrate, based on a recently published automatic adaptive thresholding method, the need for a more sophisticated method than simple thresholding to address this problem.

A. Patient Mammograms

The method has been tested on 60 studies selected from our database. Each study had two mammographic projections—CC and MLO. These mammograms were digitized on a Lumisys scanner at a resolution of 100 microns. The population includes 30 normal studies as well as 14 studies with benign and 16 with malignant masses and calcifications. Except for the exclusion of pectoral muscles in some cases, the entire method worked automatically on all mammograms wherein all parameters required by the algorithms were selected automatically. An additional 54 mammograms were processed for a different project—to assess the effect of hormone therapy on breast density. The algorithms produced visually acceptable segmentations in all 174 mammograms. Fig. 4 demonstrates the results of application of the proposed automatic method on several mammograms. The linear correlation coefficients for the parameters TG, TG/TF, TG/AvF, TG/AB, AG, AG/AF, and AG/AB derived from the two sets of projection images were 0.967, 0.902, 0.951, 0.944, 0.959, 0.915, and 0.941, respectively. The scatter plots and the R-values of different parameters across the two different projections over 60 pairs of mammograms are shown in Fig. 5(a)–(g). In all these figures, the horizontal axis represents logarithmic value of t he estimated parameter for each mammogram at the CC projection while the vertical axis represents the same for the matching mammogram at MLO projection. Although the scatter plots display logarithmic values, the R-values of linear correlation were computed on actual values of the parameters. It may be pointed out the actual scatter in the log–log graphs appear less. However, the log–log graphs were used to present compact displays for large data ranges. The ranges of gradients and y-intercepts of the trend lines were 0.998 to 1.0095 and -0.2893 to -0.0704, respectively.

The high value of correlation coefficients indicates that our method of measurement is highly consistent between the two projection images of the same patient. The highest correlation

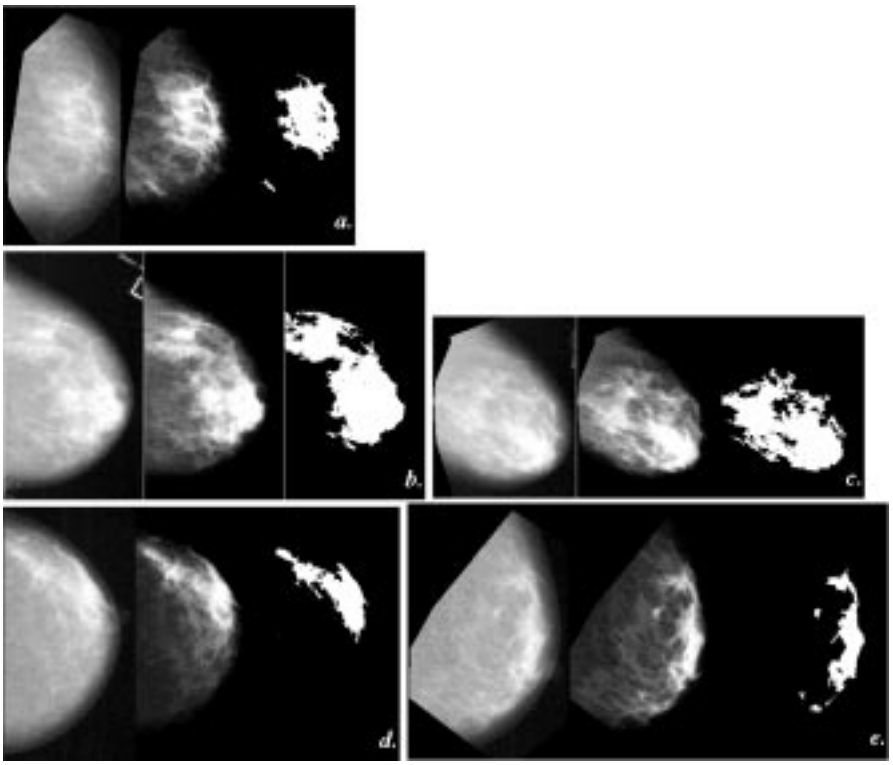

Fig. 4. Results of application of the proposed density segmentation method on several mammograms at CC and MLO projections. In each set, the original scene, the connectivity scene for the dense region and the segmented dense region are shown.

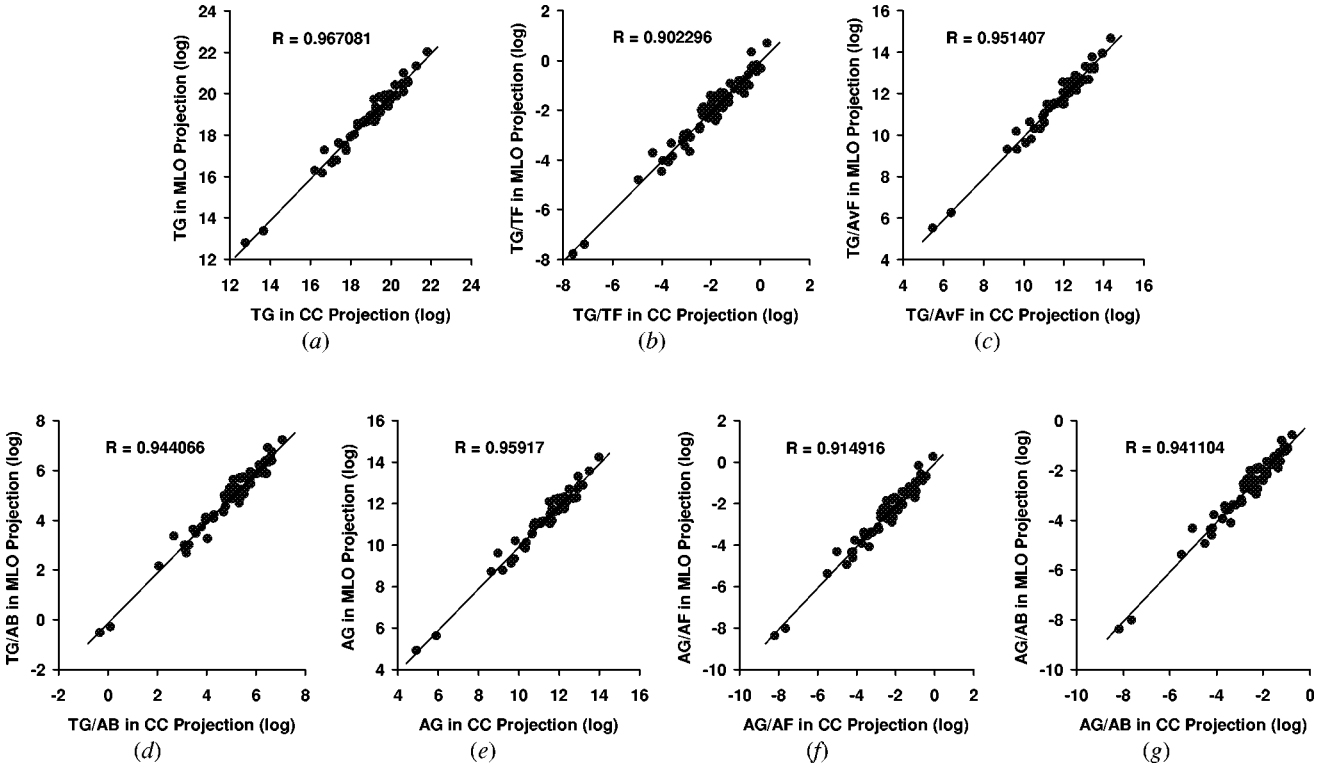

Fig. 5. (a)–(g) Scatter plots and R-values of correlation studies for different quantitative parameters computed from mammograms at CC and MLO projections. In each scatter plot, the horizontal axis indicates the logarithmic value of the parameter at CC projection while the vertical axis indicates the same at MLO projection.

is obtained for TG. Generally the parameters that use area measurements yielded lower correlations. The argument behind this may be that unless the three-dimensional (3-D) shape of the actual dense region in the breast is approximately spherical, the shapes of its CC and MLO projections may be different from each other. This may yield different area measures (AG, AF) although the total density may still be the same. To verify this hypothesis, we selected among the 60 pairs of studies a subset of

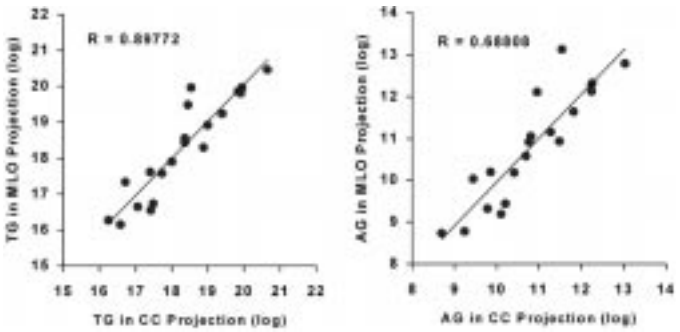

(a) (b)

Fig. 6. (a), (b) Scatter plots and R-values of correlation studies of TG and AG for a set of 20 studies with quite different shape at different projection. In each scatter plot, the horizontal axis indicates the logarithmic value of the parameter at CC project ion while the vertical axis indicates the same at MLO projection.

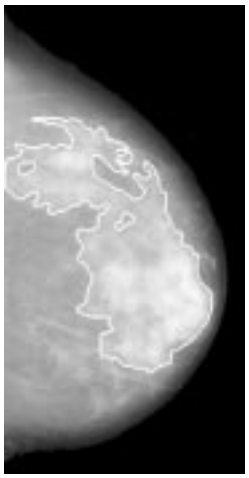

Fig. 7. An example of manual outlining. The border of the dense region is shown bright.

20 pairs in which the shapes of projections of the same breast in CC and MLO appeared quite different. For this subset, we then computed the correlation coefficients. The coefficients for TG and AG for this subset were 0.898 and 0.68, respectively. The scatter plot for this experiment is shown in Fig. 6(a) and (b). To estimate statistical significance of the difference of the correlation coefficients for these two populations, we used the Fisher's Z-transformation test [31]. The p-value was 0.036 245 showing that the difference in the correlation coefficients is statistically significant. However, the actual data were skewed and after removing the stray observations the p-value rose to 0.361 511 indicating that the difference between the correlation coefficient of TG and AG was not significant. The primary reason for this non significant difference may be the high nonlinearity between the total length in 3-D of the tissue intercepted by a beam of X-ray and the outcoming energy. If this nonlinearity is corrected for with a knowledge of the length of interception, then we believe that TG and related parameters will correspond more accurately to actual total density than the area-based parameters.

B. Comparison with Manual Outlining

A major difficulty in validating a density quantification method is how to generate the truth. Creation of a realistic

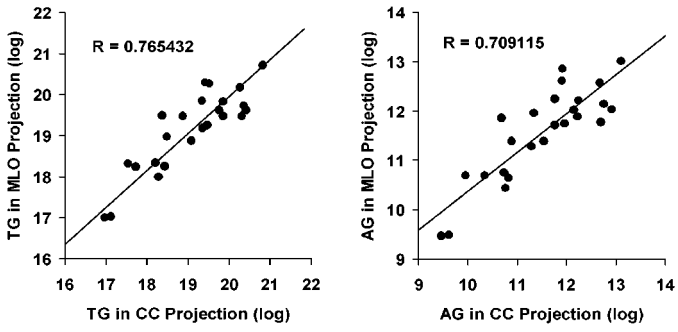

(a) (b)

Fig. 8. (a) (b) Scatter plots and R-values of correlation studies for the parameters TG and AG computed from mammograms at CC and MLO projections. In each scatter plot, the horizontal axis indicates the logarithmic value of the parameter at CC projection while the vertical axis indicates the same at MLO projection.

TABLE I
A LIST OF INTERACTIVELY AND ADAPTIVELY SELECTED THRESHOLDS TO DELINEATE MAMMOGRAPHIC DENSITIES FOR 30 MAMMOGRAMS. FIRST COLUMN: INTERACTIVELY SELECTED THRESHOLDS BY AN EXPERT MAMMOGRAPHER. SECOND COLUMN: ADAPTIVELY SELECTED THRESHOLDS USING A RECENTLY PUBLISHED METHOD

Patient number	Interactive threshold	Adaptive threshold	Patient number	Interactive threshold	Adaptive threshold
1	1846	1225	16	2175	1636
2	2030	1274	17	2108	1458
3	2098	1544	18	1952	1332
4	1895	1222	19	2098	1407
5	2039	1493	20	1816	856
6	2060	1173	21	1860	1440
7	2291	1625	22	1875	1286
8	2272	1528	23	1992	1365
9	2091	1171	24	2056	1400
10	1965	1132	25	2168	1691
11	1789	1116	26	2274	1777
12	1857	1181	27	1827	1295
13	2228	2081	28	2053	1568
14	2096	1943	29	1748	1401
15	2227	1718	30	2004	1549

physical breast phantom with known volume of dense tissue with realistic shape and distribution is a research topic of its own. In this paper, we have used manual outlining of dense regions by an expert mammographer to provide a surrogate of this truth. The outlining was performed using a computerized freehand drawing tool on digitized mammograms as supported by 3DVIEWNIX [26]. An example of manual outlining is presented in Fig. 7. The task of manual outlining is difficult, quite ill-defined, and has its own limitations in terms of definition and inter and intraoperator variability. Additionally, we observed that the correlation of the density parameters computed from manual outlining is lower than that using the proposed method. Twenty five pairs of mammograms were randomly selected

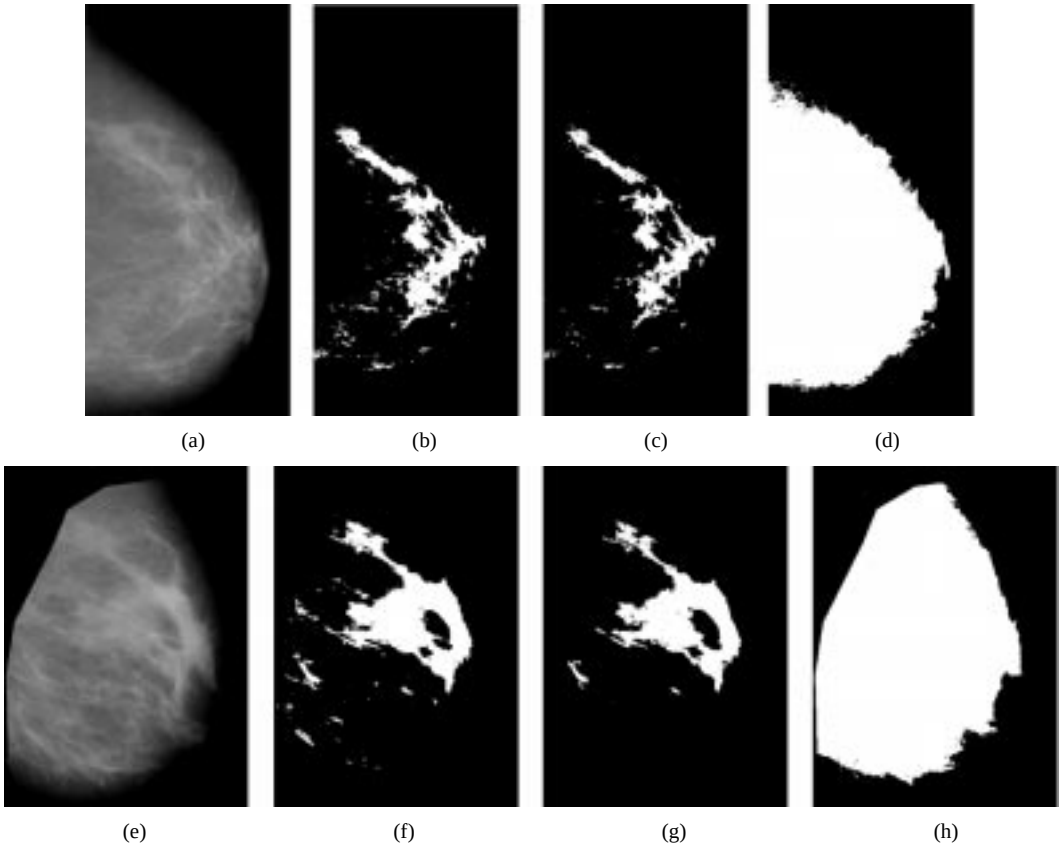

Fig. 9. Illustration of delineation of mammographic dense regions using different methods. (a), (e) Two original mammograms. (b), (f) Segmented dense regions from the mammograms in (a) and (e), respectively, using interactive thresholding. (c), (g), Same as (b), (f) but using the proposed method. (d), (h), Same as (b), (f) but using the an adaptive thresholding method.

from our data set of 60 pairs of mammograms. Dense regions in each mammogram were manually outlined by the same expert and the parameters TG and AG were computed over the delineated regions. The linear correlation coefficients for TG and AG were 0.765 and 0.709, respectively. The scatter plots and the R-values of these two parameters across the two projections over these 25 pairs of mammograms are shown in Fig. 8(a) and (b).

While the correlation of different density parameters computed by the proposed method is demonstrated in the previous section, the purpose of the experiment described here is to show that the disagreement of the results produced by the automatic method with those of manual outlining is within the limitation range of the second method itself. Twenty five mammograms were randomly selected from our data set of 120 mammograms. Dense regions in each of these mammograms were manually outlined by the same expert at two different time instants (with a gap of two days). Also, the dense regions were segmented in each mammogram using the proposed method. For any two segmentation methods and for each mammogram, a percent area mismatch measure, AM, was computed. Let X and Y be two sets of pixels segmented as dense regions using the two segmentation methods in a mammogram. Then percent area mismatch $AM(X, Y)$ was computed as $|X \,\mathrm{EOR}\, Y|/((|X| + |Y|)/2) \times 100$. Thus, for any two methods we obtained 25 different values for AM from 25 mammograms and calculated the mean M and standard deviation σ of these 25 values. Finally, the 95% confidence interval was computed. The 95% confidence interval of AM for manual segmentation at different time instants was $[0, 22.81]$ and that for manual and the automatic method was $[0, 18.14]$. This shows that the disagreement of delineation using the proposed method with manual outlining is within the range of variability of the latter method itself.

C. Simple Thresholding

To evaluate a fixed thresholding method, we randomly selected 30 mammograms from our database. A trained mammographer interactively selected a threshold for each mammogram by using 3DVIEWNIX [26] to delineate th e dense regions. The thresholds for the 30 mammograms are listed in Table I and interactively segmented dense regions for two mammograms are shown in Fig. 9(b) and (f); the original mammograms are shown in Fig. 9(a) and (e), respectively. Corresponding segmented dense regions using the proposed method are presented in Fig. 9(c) and (g). In each of these two examples, segmented dense regions using the proposed method are visually close to those obtained interactively. High variability in the interactively selected thresholds, as seen in Table I, suggests that fixed thresholding is not possible in this application. Also, we tested a recently published adaptive thresholding method [30] on the same set of 30 mammograms with the idea that a good agreement of the adaptively selected thresholds with those selected interactively would suggest the usability of the method to automatically delineate mammographic dense regions. We selected this particular method as this is a recent method and the authors have compared it with several other earlier methods and have established

its superiority. Since the task is to segment the breast regions into fatty and dense regions, all computations were confined to the breast region only. The computed adaptive thresholds are listed in Table I which shows that the adaptive thresholds are far from agreement with the corresponding interactively selected thresholds. Moreover, we observed that the adaptive thresholds are consistently lower than the interactive thresholds. A reason for this may be that the algorithm attempts to fit two Gaussian distributions to the intensity histogram and has a tendency to uniformly divide the two regions in terms of their area. This demonstrates that a sophisticated method, such as the one presented in this paper, is needed for the automatic quantification of densities in mammograms.

V. Conclusion

A near automatic method for quantification of breast density from digitized mammograms has been developed and tested on 87 pairs of patient mammograms. This method works automatically except for the exclusion of projected pectoral muscles. It consists of the following steps: separation of the breast from the background, creation of a fuzzy connectivity scene for the dense region, segmenting this connectivity scene using an automatic threshold selection method, and then computing various parameters that characterize total breast density. A set of density and area related parameters has been proposed and their precision in terms of their linear correlation across two different projections has been studied. The scale-based fuzzy connectivity method has been found to be very robust and effective in segmenting the mammographic images. Amount of density is considered to be one of the strongest risk factors for breast cancer. Automatic, repeatable, and consistent breast density quantification from digitized mammograms is practical using the proposed method. The correctness of the proposed density quantification method has been studied in two ways—1) showing high R-values of linear correlation between the two projections (CC, MLO) of the various parameters computed over segmented dense and fatty regions and 2) demonstrating the agreement between delineations using the proposed method and using manual outlining to be within the range of variability of the second method. The method removes the subjectivity inherent in interactive threshold selection techniques currently used. By comparing with a recently published adaptive thresholding method, we have demonstrated the failure of such simpler techniques and the need for more sophisticated strategies to automatically and routinely segment dense regions. The ability of the computed density parameters in evaluating risk is currently being investigated at our institution.

A comparison between the mammographic density parameter taking into account the original intensities and that considering just the segmented area has been carried out. The motivations behind this consideration was that unless the 3-D shape of the actual dense region in the breast is approximately spherical, the shapes of its CC and MLO projections may be quite different from each other while intensity based parameters would better capture the thickness and volume of the dense region using intensity information. For 60 pairs of mammograms at CC and MLO projections, generally the parameters that use area measurements yielded lower correlations. To verify this argument, we selected among the 60 pairs of studies a subset of 20 pairs in which the shapes of projections of the same breast in CC and MLO appeared quite different and difference in the correlation coefficients was statistically significant. However, when the skewness of data was removed by removing stray observations, there was no significant difference in correlation coefficients of purely area based parameters and those taking into account actual mammographic intensities. The primary reason behind this disagreement may be the high nonlinearity between the total length in 3-D of the tissue intercepted by a beam of X-ray and the outcoming energy. Another hurdle in using intensity related parameters originates from the fact that the values of these parameters do not indicate the actual volume of dense regions. This is because, actual intensities in mammograms are dependent on different imaging parameters such as the energy and the frequency of X-rays used, plate thickness, film characteristics and X-ray attenuation coefficients of different tissues of different patients. It will be useful in the future to resolve this problem of nonlinearity and to somehow normalize the total density parameters such that they relate to the physical volume of dense regions.

Acknowledgment

The authors would like to thank Dr. L. Toto and Dr. H. L. Kundel for the digitized mammographic data set.

References

[1] J. N. Wolfe, "Breast pattern as an index of risk for developing breast cancer," *AJR*, vol. 126, pp. 1130–1139, 1976.

[2] ——, "Breast parenchymal patterns and their changes with age," *Radiology*, vol. 121, pp. 545–552, 1976.

[3] E. Warner *et al.*, "The risk of breast-cancer associated with mammographic parenchymal patterns: A meta-analysis of the published literature to examine the effect of method of classification," *Cancer Detect. Prevent.*, vol. 16, pp. 67–72, 1992.

[4] A. M. Oza and N. F. Boyd, "Mammographic parenchymal patter ns: A marker of breast cancer risk," *Epidemiologic Rev.*, vol. 15, pp. 196–208, 1993.

[5] J. N. Wolfe, "Risk for breast cancer development determined by mammographic parenchymal pattern," *Cancer*, vol. 37, pp. 2486–92, 1976.

[6] N. F. Boyd, J. W. Byng, R. A. Jong, E. K. Fishell, L. E. Little, A. B. Miller, G. A. Lockwood, D. L. Tritchler, and M. J. Yaffe, "Quantitative classification of mammographic densities and breast cancer risk: Results from the Canadian national breast screening study," *J. Nat. Cancer Inst.*, vol. 87, pp. 670–675, 1995.

[7] M. Moscowitz, P. Gartside, and C. McLaughlin, "Mammographic patterns as markers for high-risk benign breast disease and incident cancers," *Radiology*, vol. 134, pp. 293–5, 1980.

[8] J. N. Wolfe, A. F. Saftlas, and M. Salane, "Mammographic parenchymal patterns and quantitative evaluation of mammographic densities: A case control study," *Amer. J. Roentgenol.*, vol. 148, pp. 1087–92, 1987.

[9] J. K. Udupa, L. Wei, Y. Miki, and R. I. Grossman, "A system for comprehensive analysis of multiple sclerosis lesion load based on MR imagery," *SPIE Proc.*, vol. 3031, pp. 610–618, 1997.

[10] J. K. Udupa, L. Wei, S. Samarasekera, Y. Miki, M. A. van Buchem, and R. I. Grossman, "Multiple sclerosis lesion quantification using fuzzy connectedness principles," *IEEE Trans. Med. Imag.*, vol. 16, pp. 598–609, Oct. 1997.

[11] Y. Miki, R. I. Grossman, J. K. Udupa, M. A. van Buchem, L. Wei, M. D. Philips, U. Patel, J. C. McGown, and D. L. Kolson, "Differences between relapsing remitting and chronic progressive multiple sclerosis as determined with quantitative MR imaging," *Radiology*, vol. 210, pp. 769–774, 1999.

[12] Y. Miki, R. I. Grossman, J. K. Udupa, L. Wei, M. Polansky, L. J. Mannon, and D. L. Kolson, "Relapsing-remitting multiple sclerosis: Longitudinal analysis of MR images—Lack of correlation between changes in T2 lesion volume and clinical findings," *Radiology*, vol. 213, pp. 395–399, 1999.

[13] A. Kumar, W. Bilker, J. K. Udupa, and G. Gottlieb, "Late onset minor and major early evidence for common neuroanatomical substrates detected by using MRI," in *Proc. National Academy of Science*, vol. 95, 1998, pp. 7654–7658.

[14] B. L. Rice, Jr. and J. K. Udupa, "Clutter-free volume rendering for magnetic resonance angiography using fuzzy connectedness," *Int. J. f Imag. Syst. Technol.*, vol. 11, pp. 62–70, 2000.

[15] J. K. Udupa, J. Tian, D. C. Hemmy, and P. Tessier, "A pentium-based craniofacial 3-D imaging and analysis system," *J. Craniofacial Surg.*, vol. 8, pp. 333–339, 1997.

[16] S. M. Lippman, T. L. Bassford, and F. L. Meyskens, Jr., "A quantitatively scored cancer-risk assessment tool: Its development and use," *J. Cancer Edu.*, vol. 7, pp. 15–36, 1992.

[17] R. T. Chlebowski *et al.*, "Breast cancer chemoprevention tamoxifen: Current issues and future prospective," *Cancer*, vol. 72, pp. 1032–7, 1993.

[18] J. M. Boone, K. K. Lindfors, C. S. Beatty, and J. A. Selbert, "A breast density index for digital mammograms based on radiologists' ranking," *J. Digital Imag.*, vol. 11, pp. 101–115, 1998.

[19] J. W. Byng, N. F. Boyd, L. Little, G. Lockwood, E. Fishell, R. A. Jong, and M. J. Yaffe, "Symmetry of projection in the quantitative analysis of mammographic images," *Eur. J. Cancer Prevent.*, vol. 5, pp. 319–327, 1996.

[20] G. Ursin, A. Melvin, A. Astrahan, M. Salane, Y. R. Parisky, J. G. Pearce, J. R. Daniels, M. C. Pike, and D. V. Spicer, "The detection of changes in mammographic densities," *Cancer Epidemiol. Biomarkers Prevent.*, vol. 7, pp. 43–47, 1998.

[21] Z. Huo, M. L. Giger, O. I. Olopade, and S. A. Cummings, "Computerized analysis of parenchymal patterns for the assessment of breast cancer risk," *Suppl. Radiology, RSNA*, vol. 209(P), p. 354, 1998.

[22] J. Suckling, D. R. Lewis, and S. G. Blacker, "Parenchymal delineation by human and computer observers," presented at the 2nd Int. Workshop Digital Mammography, A. G. Gale *et al.*, Eds., York, U.K., 1994.

[23] R. Highnam, M. Brady, and B. Shepstone, "A representation for mammographic image processing," *Med. Image Anal.*, vol. 1, pp. 1–18, 1996.

[24] J. K. Udupa and S. Samarasekera, "Fuzzy connectedness a nd object definition: Theory, algorithms, and applications in image segmentation," *Graphical Models Image Processing*, vol. 58, pp. 246–261, 1996.

[25] P. K. Saha, J. K. Udupa, and D. Odhner, "Scale-based fuzzy connected image segmentation: Theory, algorithms, and validation," *Comput. Vis. Image Understanding*, vol. 77, pp. 145–174, 2000.

[26] J. K. Udupa, D. Odhner, S. Samarasekera, R. J. Goncalves, K. Iyer, K. Venugopal, and S. Furuie, "VIEWNIX: A open, transportable, multidimensional, multimodality, multiparametric imaging system," *Proc. SPIE*, vol. 2164, pp. 58–73, 1994.

[27] A. X. Falcão, J. K. Udupa, S. Samarasekera, and S. Sharma, "User-steered image segmentation paradigms: Live wire and live lane," *Graphical Models Image Processing*, vol. 60, pp. 233–260, 1998.

[28] M. Tabb and N. Ahuja, "Multiscale image segmentation by integrated edge and region detection," *IEEE Trans. Image Processing*, vol. 6, pp. 642–655, May 1997.

[29] T. Lindeberg, *Scale-Space Theory in Computer Vision*. Boston, MA: Kluwer, 1994.

[30] C. K. Leung and F. K. Lam, "Maximum segmented image information thresholding," *Graphical Models Image Processing*, vol. 60, pp. 57–76, 1998.

[31] R. F. Woolson, *Statistical Methods for the Analysis of Biomedical Data*. New York: Wiley, 1987.

[32] T. S. Curry, J. E. Dowdey, and R. C. Murry, Jr., *Christensen's Introduction to the Physics of Diagnostic Radiology*. Philadelphia, PA: Lea & Febiger, 1984.